A Large Eddy Simulation of the Fenestron® at high blade pitch angle

Marino Morgane*, Gourdain Nicolas †, Boussuge Jean-François§, Legras Guillaume ‡ and Alfano David ‡

*PhD Candidate,

morgane.marino@airbus.com

Airbus Helicopters S.A.S, 13725 Marignane, France and CERFACS, 31057 Toulouse, France

†Professor, Department of aerodynamics, energetics and propulsion

ISAE Sup'Aero, 31400 Toulouse, France

§Senior Research Engineer, CERFACS, 31057 Toulouse, France

‡Engineer, Aerodynamics department

Airbus Helicopters S.A.S, 13725 Marignane, France

ABSTRACT:

The helicopter manufacturers face a great challenge by extending the limit of the flight envelop for adapting their rotorcrafts to changing customer needs. For supporting further developments, the recent progress in Computational Fluid Dynamics (CFD) enable a better understanding of the flow physics especially in the case of complex geometries like the Fenestron®. This paper proposes a first Large Eddy Simulation (LES) performed on a full scale Dauphin Fenestron®. The objective is to better understand the turbulent flows especially for high blade pitch angle where the rotor blade can encounter massive boundary-layer separations. A comparison between a steady state RANS and a LES is achieved to characterize the effect of turbulence modeling on the flow predictions. Both approaches are compared with experimental data to evaluate the capability of the numerical simulations to estimate both global performance (thrust and power) and local flows (static pressure at the shroud and radial profiles inside the vein). Global performance are correctly predicted by RANS and LES. The LES approach accurately predicts the flow in the vicinity of the rotor blade, with a particular interest for the tip-leakage flow. In this region a qualitative analysis of the two solutions highlights different vortex roll-up behaviors.

1. ABBREVIATION AND SYMBOL

1.1 Abbreviation

CFD	Computational Fluid Dynamics
CFL	Courant-Friedrichs-Lewy
DTS	Dual time step
elsA	Ensemble logiciel de simulation aerodynamique
JST	Jameson Schmidt Turkel
LES	Large Eddy Simulation
RANS	Reynolds-Averaged Navier-Stokes
SST	Shear Stress Transport
WALE	Wall-Adapting Local Eddy-Viscosity

1.2 Symbol

F_T	Fenestron® thrust	[DaN]
Fp	Fenestron® power	[kW]
h	Radial position in the vein	[m]
H	Height of the vein	[m]
h/H	Normalized radial position	[-]
k	Turbulent kinetic energy	[$m^2.s^{-2}$]
p	Static pressure	[Pa]
p_∞	Ambient pressure	[Pa]
R	Fenestron® radius	[m]
Vz	Axial velocity	[$m.s^{-1}$]
y+	Non dimensional wall distance Density	[-]
x+	Non dimensional distance Density	[-]
z+	Non dimensional streamwise distance Density	[-]
ρ	Density	[$kg.m^{-3}$]
ω	Frequency of turbulence kinetic energy	[Hz]
Ω	Rotational speed	[$rad.s^{-1}$]
V_{TIP}	Blade tip velocity, RΩ	[$m.s^{-1}$]
V_∞	Impose velocity in the inflow direction	
CFT	Fenestron® Thrust coefficient (1) $\frac{F_T}{\rho\pi R^2 V_{tip}^2}$	[-]
CFP	Fenestron® Power coefficient (2) $\frac{F_P}{\rho\pi * R^2 V_{tip}^3}$	[-]
Cp	Pressure coefficient (3) $(\frac{p-p_\infty}{\frac{1}{2}\rho {V_{tip}}^2})$	[-]
ΔT	Non dimensional time $\Delta T = \frac{time * Vtip}{R}$	[-]

2. INTRODUCTION

With experience acquired since the conception in 1970's [1]-[2] by the engineering department of Sud-Aviation, the Fenestron® has become a trademark for Airbus Helicopters on light-to-medium helicopters. Thanks to extensive flights and Research and Development, the Fenestron® improves customers' safety and complies with new noise standards. The main function of the Fenestron® is to provide the necessary thrust to counterbalance the torque of the main rotor. For it crucial anti-torque function, the sizing of the Fenestron® is a key point when designing a helicopter. For future shrouded rotor design, a comprehensive analysis of the flow is needed to accurately predict the aerodynamic properties of such complex geometry.

Due to the relative motion between fixed (shroud-stator) and rotating parts (rotor) the internal flow of the Fenestron® is three-dimensional, turbulent and unsteady. Like in most turbomachines [3], secondary flows exist in the Fenestron®, such as the tip leakage flow induced by the clearance between the rotor and the shroud. Moreover since the flight domain of a helicopter is wide, non-ideal conditions are encountered during missions. Under collector side wind conditions, the Fenestron® operates at high blade pitch angle. The more the wind velocity increases, the less the rotor generates thrust as it is reported by [4]. In this lateral flight condition, flow separations behind the shroud and the hub have been highlighted by [5].

For supporting experimental campaign [7]-[9], the Computational Fluid Dynamics (CFD) is an alternative way to provide a better understanding of the flow physics in this system. A literature review of the Fenestron® simulation is proposed in [10]. Three numerical approaches are proposed to compute the flow of the shrouded rotor; the first one is the use of an actuator disk to represent the rotor while preserving a high fidelity helicopter geometry [11]-[12]; the second approach consists in reducing the domain to one blade passage model [13] and the third one consists in computing the whole geometry of the helicopter accounting for rotating parts [14]. The latter approach leads to a high computational cost. The common point of the three approaches is the use of the Reynolds-Averaged Navier-Stokes (RANS) equation which requests turbulence models for closure to represent the effects of turbulence on the mean-flow properties. A previous work [10] has been done in hover conditions. It shows that for low rotor stress conditions (for a blade pitch angle from -10° to +35°), if the grid is set up with a sufficient care, numerical parameters has no impact on the prediction of the Fenestron® performance. However, beyond +35°, local phenomenon appears especially in the vicinity of the blade tip where the turbulence modelling has a major effect on the flow prediction. These observations point out the need to evaluate the capability of different turbulence models to represent the flow in this complex region at high blade pitch angles.

An alternative way to the RANS approach is the Large Eddy Simulation (LES), for which large scales are simulated and scales smaller than the mesh-cell sizes are modelled by a sub-grid model. Because of the high Reynolds number of the flow, the complex phenomenon due to the interactions between rotors and fuselage, and the complexity of the geometry, the helicopter is a challenging application for LES. Therefore, most works deal with a Detached Eddy Simulation (DES) by computing the whole geometry [15] or focusing on some helicopter parts like the rotor [16]. For complete helicopter geometry, a comparison between RANS and DES approaches [15] point out the better capability of DES to cope with massive flow separations in forward flight. DES and LES also lead to a better understanding of flow interactions by resolving accurately the main rotor wake [16] as well as the blade-tip vortex [17]. For turbomachinery, LES also demonstrates its capability to predict laminar-to-turbulent transition for rotor at high Reynolds number [18].

The main objective of this study is to address a comprehensive analysis of the flow of the Fenestron®. To validate the RANS/LES comparison, numerical predictions are compared to bench test measurements on a full scale Dauphin Fenestron® [7]. The CFD approach is based on the single blade passage proposed by Mouterde *et al.* in [9].

As reported in the literature [19], there are four main sources of errors when computing a numerical simulation when comparing numerical predictions with experimental data. The first one is the reliability of the geometry, the second one is the boundary conditions used; the third one is the adequacy between the numerical scheme and the mesh grid quality and the fourth one is the turbulence modelling. This paper proposes a comparison between RANS and LES approaches on a reliable Dauphin Fenestron® geometry and evaluates the influence of the turbulence modelling.

This paper is organized in four parts. The first part of the study exposes the two turbulence approaches used for the simuation. The second part details the investigated test case and the experimental data base. The computational set up is then described. Finally, the fourth part focuses on a quantitative and qualitative analysis of the aerodynamics of the Fenestron®. Then conclusions are drawn.

3. THE TWO NUMERICAL METHODS

The hazardous and erratic behavior of the turbulence remains a hard issue to model. In numerical simulation, only the Direct Numerical Simulation resolves all the turbulent scales without using any turbulence model. The spatial discretization to represent the whole turbulent patterns scales as $\mathrm{Re}^{9/4}$ number of points. For example, applying a DNS on the Fenestron® geometry needs a grid refinement that scales as 10^{13} points. It is thus currently unaffordable to realize a DNS for such a problem. Steady or unsteady RANS simulations are usually performed on helicopter industrial configuration. As mentioned, LES is a potential solution to simulate the largest turbulent scales of the flow, but its application to the Fenestron® geometry suffers from a lack of validation.

3.1 The RANS approach

The RANS approach is based on the statistical average of the Navier-Stokes equations. The mean flow is predicted and all turbulent scales are modeled. Its cost and robustness make it an appropriate solution for industrial applications as well as parametric studies.

The enclosed problem can be solved with a first order model. In this case, different turbulence models are available. The one selected for this study is the two transport equations model of k-ω Kok [20] with the Shear Stress Transport (SST) correction. The k-ω turbulence model is based on one transport equation for the kinetic turbulent energy k (4) and one transport equation for the frequency of the turbulence ω (5). The SST correction proposed in [21] avoids the delay in the prediction of adverse pressure-gradient effects. For high rotor stress conditions, the adverse pressure gradient is important near the collector and the blade tip as it was described by [10]. This correction is thus helpful for the flow prediction at high pitch angles. In the present case, the flow predicted in the current RANS simulation is assumed to be fully turbulent as the Reynolds number base in the blade chord is above 10^6.

$$(4) \quad \frac{\partial k}{\partial t} + U_k \frac{\partial k}{\partial x_k} = P - \beta' k\omega + \frac{\partial}{\partial x_k}\left[\left(\nu + \frac{\nu_t}{\sigma_k}\right)\frac{\partial k}{\partial x_k}\right]$$

$$(5) \quad \frac{\partial \omega}{\partial t} + U_k \frac{\partial \omega}{\partial x_k} = \frac{\gamma}{\nu_t} P - \beta\omega^2 + \frac{\partial}{\partial x_k}\left[\left(\nu + \frac{\nu_t}{\sigma_\omega}\right)\frac{\partial \omega}{\partial x_k}\right]$$

Where :

$$\nu_t = \frac{k}{\omega} \; ; \; P = 2\nu_t S_{ij} S_{ij} ; \; \gamma = 0.5 \; ;$$
$$\beta = 0.075 \; ; \; \beta' = 0.09 \; ; \; \sigma_\omega = 0.5 \; ; \; \sigma_k = 0.5$$

3.2 The LES approach

The Large Eddy Simulation resolves the dynamics of the large scales and only a fraction of the turbulent movement is modelled. Large scales are conditioned by the geometry whereas small ones are more homogeneous and universal. Its principle is based on a spatial filtering of the Navier-Stokes equations. It results in a scale separation, supported by the grid local cell size which plays the role of the cut-off wave number, between the resolved scales and the one called the sub-grid scales. The role of the sub-grid model is to ensure the dissipation of the smallest scales. Therefore, as the filter is based on the grid size, the solution dependents on the grid refinement and the mesh quality as described by Spalart [22]. To estimate the grid refinement, Piomelli [23] divides the boundary layer into two regions; the outer part of the boundary layer and the inner layer. The issue is the variation of the boundary layer with the Reynolds number. At high Reynolds number, the physical eddies of the flow decline more rapidly than the thickness of the boundary layer. To solve accurately the inner part, the grid refinement must be significant: Chapman [24] estimated the number of points varying to $Re^{1.8}$ in this region. For the outer layer, the grid dependency is proportional to $Re^{0.4}$.

Among various sub-grid models, it is proposed to use the Wall- Adapting Local Eddy-Viscosity (WALE) model developed by Nicous and Ducros [24]. It is based on the Smagorinsky approach but an operator is defined to take into account the strain tensor $\bar{S}$ and the rotational rate. It also changes the behavior of the model near the wall to be compliant with a zero turbulent viscosity ($\nu_t = 0$) at the wall. Moreover, the WALE model is invariant to any coordinate translation or rotation.

$$(6) \quad \nu_t = (C_\omega \Delta)^2 * \frac{\overline{\overline{OP1}}}{\overline{\overline{OP2}}}$$

Where :

$$C_\omega = 0.5 \; ; \; \Delta = \sqrt[3]{\Delta x \Delta y \Delta z}$$

$\frac{\overline{\overline{OP1}}}{\overline{\overline{OP2}}}$ operator in time and space homogeneous to a frequency.

4. INVESTIGATED GEOMETRY AND EXPERIMENTAL CAMPAIGN

A Fenestron® is composed of a shrouded rotor and topped with a large vertical fin, as described on the Figure 1 and Figure 3. The shroud is composed of a collector with rounded lips, a cylindrical zone at the blade passage and a conical diffuser. The hub is supported by three arms or a stator row. The gearbox, located inside the hub, provides power to the rotor and controls the blade pitch angle. The rotor pitch drives the rotor thrust of the Fenestron®. In hover flight, the rotor leads the flow from the collector to the diffuser, creating the shroud effort. The thrust of the Fenestron® is thus composed by the shroud thrust and the rotor thrust.

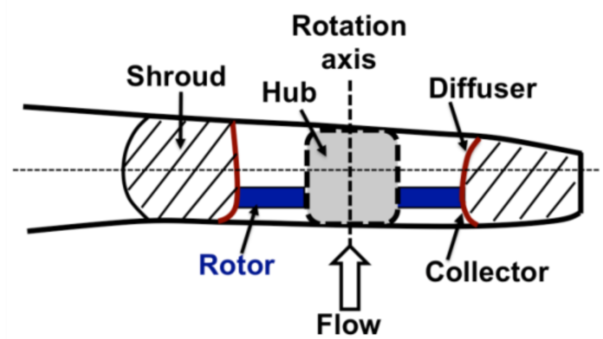

Figure 1 : Overview of the Fenestron® principle

4.1 Experimental data base

The experimental case is the Dauphin Fenestron® experimentally tested by Morelli and Vuillet [7] in 1985. Among the different configurations described in [7], the reference case is retained. It is based on a rotor with 11 equally-spaced blades and a hub supported by three arms. A balance (with an accuracy of 1%) and a torque system (with an accuracy of 0.5%) are used to measure thrust and power. As illustrated in Figure 2, the local flow is evaluated by measuring the static pressure with 32 steady sensors located along the duct vein. The flow is also characterized upstream (plane 1) and downstream the rotor (plane 2 and 3) at several radial locations with a 5-hole probe. Only a time average of the probe values is available.

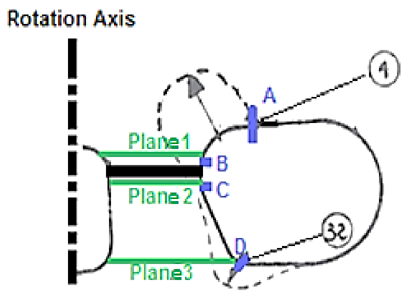

Figure 2: Radial profiles extracted on plane 1 to 3 and static pressure measurements situated from A to D at the shroud (from Morelli and Vuillet [7])

4.2 Investigated test case

Under collector side-wind condition, the rotor evolves at high rotor stress conditions which correspond to high blade pitch angle. Previous work in hover condition [10] pointed out a significant tip-leakage flow. Moreover discrepancies between the RANS simulation and the experimental data in the vicinity of the blade rotor were highlighted. The influence of the turbulence model appears at the blade pitch angle of +35° on the global performance such as the thrust pitch polar. Therefore, a blade pitch angle of +35° has been considered in the rest of the study.

Regarding the cost of a LES calculation (section 3.2) for a complete Fenestron®, the simulated domain is reduced to a single blade passage. An evaluation of the blade passage model by [10] gives good results on the prediction of global and local performance. Thanks to 11 equally-spaced blades, the main hypothesis of the model is based on the periodicity of the solution. A sketch of the geometry used for the simulation is described on Figure 3. The simulated part is highlighted in red. Numerical calculations are performed at a rotation speed of Ω=100%. The mean Reynolds number, based on the blade chord, is around $1.2\text{x}10^6$.

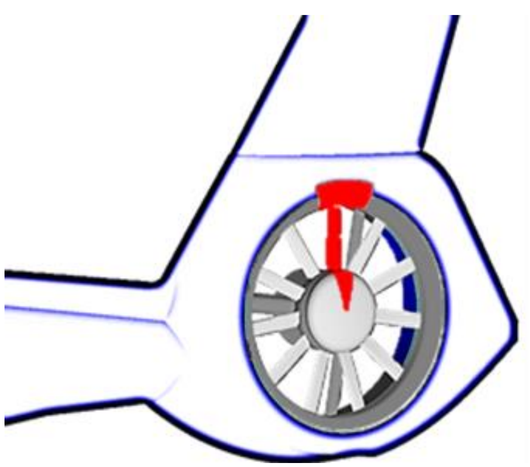

Figure 3 : 3D sketch of the 3D Fenestron® geometry

5. COMPUTATIONAL SET UP

5.1 The flow solver

The governing equation of the problem is the Navier-Stokes equations, which have been resolved with the *elsA* software, developed by ONERA [25]. This solver is a multidisciplinary object-oriented code, dedicated to aerodynamic flows. It is based on cell-centered finite volume formulation and rely on multi-block structured meshes. Both internal and external tridimensional flows are simulated by the code.

5.2 Numerical parameters

For RANS and LES approaches, the study is performed with the second-order centered scheme proposed by Jameson and Turkel [26] for convective fluxes. To stabilize the JST scheme, an artificial viscosity term is added with a scalar artificial viscosity. The linear fourth order dissipation term k4 is set to 0.016. Diffusive fluxes are calculated with a second order centered schemes.

For the unsteady part of the proposed study, the time-marching is performed by using a second order implicit time integration scheme based on the backward Euler scheme and a scalar lower-upper symmetric successive over-relaxation (SSOR) method proposed by Youn and Jameson [29]. This time-marching method is coupled with a second-order dual time stepping method (DTS) [30]. For implicit unsteady simulation, the choice of the time step is a key point for resolving turbulent flow patterns. The local Courant-Friedrichs-Lewy number (CFL) is determined by the local velocity, the time step and the grid resolution chosen for the simulation. As for the grid resolution that determines the size of the resolved structures, the maximum computed frequencies are discriminated by the time step. Because, the flow is solved in the reference frame of the rotor, the characteristic frequencies are the frequency of the blade wake, the one of the tip leakage flow and potential boundary layer transition or detachment. A non-dimensional time step $\Delta t=1.75.10^{-3}$ is chosen for the simulation (it corresponds to 3,600 times steps to discretize one rotor rotation). The inner loop is described by 10 sub-iterations to get at least a reduction of two orders of magnitude for conservatives flux.

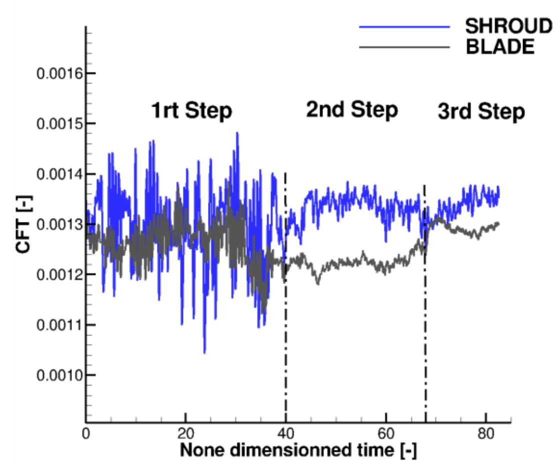

Figure 4 : Thrust convergence of the LES approach for the blade and shroud elements

The LES calculation is initialized with a RANS computation and 30 rotations are necessary to reach the targeted Δt. A first simulation of 20 revolutions is carried with $\Delta t' = 100\Delta t$. A second step consisted in 10 revolutions with $\Delta t' = 10\Delta t$. Finally, 4 revolutions are simulated with Δt. The convergence of the rotor and shroud thrusts is presented on Figure 4.

5.3 Meshing strategy

The complexity of the mesh comes from the gap between the rotor and the shroud, the rotor blade-root and the blade twist angle. The usual method for Fenestron® computations is the Chimera approach. It consists in meshing separately the fixed and the rotating parts. Nevertheless, the blade-wake propagation is influenced by the order of the chimera interpolation [10]. To preserve the wake, a high-order chimera interpolation [28] or a no-match approach can be used. In this study the no-match approach is selected. It consists in segregating the domain in two meshes separated by a no-match plane. To avoid filtering through the plane, the sizes of the cells are homogeneous on both sides. Special attention was paid to the location of the two no-match planes, which are described on Figure 5. The first plane is located before the cylindrical zone, at the end of the collector geometry. The second no-match plane is located behind the blade, at the end of the cylindrical zone. As defined on Figure 5, the rotational axis is aligned with the inflow direction; the blade pitch axis extends from the root to the tip, the origin being at the center of the hub.

As the study focuses on the interactions between the shroud and the blade, efforts were made on the blade tip gap and the streamwise direction. To reach the quality standards for a LES approach, the dimensionless wall distance is set to $y^+ \sim 0.5$. The mean aspect ratio between the streamwise normal direction and the wall normal direction is approximately 350. The mean aspect ratio between the spanwise normal direction and the wall normal direction is approximately 700. The mesh stretching in the spanwise direction is important. Nevertheless, previous RANS work [10] highlighted the low dependence of the solution to the grid refinement in the spanwise-blade direction. The mesh density is described in table 1 and 2. The wall-normal first cell is sized to 1μm.

The total size of the domain is around 20-R (with R the radius of the Fenestron®) around the shroud geometry. To avoid flow recirculation near the limit of the simulated box a buffer zone is done with a coarse grid.

The whole domain contains 8520 blocks and 73 million of grid cells. The quality of the mesh at h/H=0.8 can be observed on Figure 6. The grid refinement on the blade is illustrated on Figure 7. In order to compare RANS and LES solutions, both calculations are performed on the same mesh.

Point distribution between the no-match planes	Mesh (points)
Gap	97
Blade span (from the hub to the shroud)	277
Main blade streamwise direction	332
Azimuthal direction	125

Table 1: Mesh density around the blade

Point distribution inside the vein	Mesh (points)
Tip height	97
Blade height	275
Main blade streamwise direction	623
Azimuthal direction	121

Table 2 : Mesh density into the vein

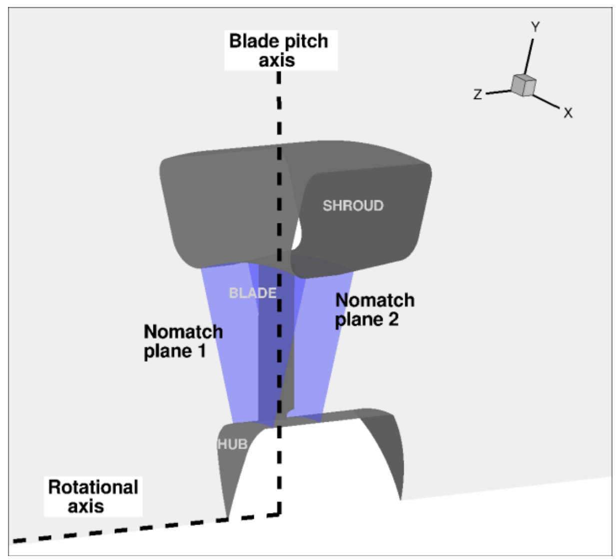

Figure 5 : Axi-symmetric channel model using the no-match approach

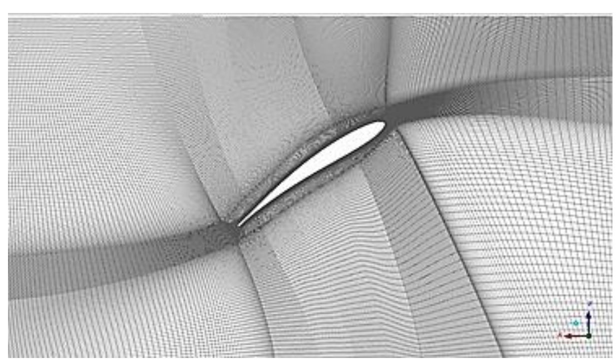

Figure 6 : Grid refinement of the blade at h/h=0.8

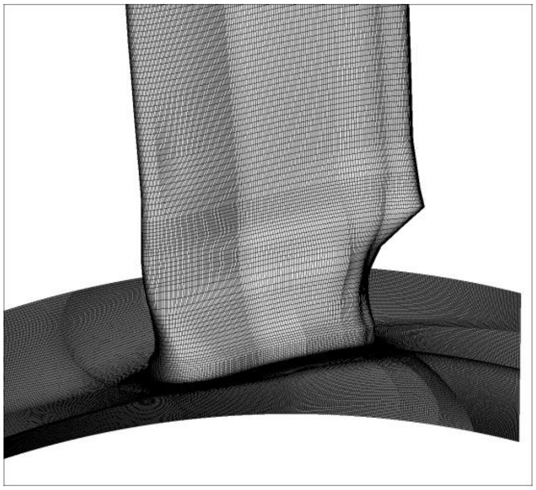

Figure 7 : Grid refinement of the blade root

5.4 Boundary conditions

As the simulated domain is reduced to an axi-symmetric channel model, periodic boundary conditions are applied on the lateral faces. The shroud, the hub and the blade walls are represented with non-slip boundary conditions. The other part of the domain is considered as the far-field. First LES calculations were carried out without any axial velocity. The size of the simulated domain (20R) was not enough to dissipate the recirculation situated near the corners. A choice was done between the expansion of the numerical domain which increases the size of the mesh and the time-computing or introducing a low axial velocity to evacuate the flow.

An evaluation of the Fenestron® performance under collector side-wind condition for a blade pitch angle of +35° was done. To ensure that the flow generated by the rotor is driven outside the numerical domain, and avoid massive recirculations, it has been chosen to impose a velocity in the inflow direction as $V\infty=1\%Vtip$. This approach modifies the total thrust of the Fenestron® by less than 0.3%.

6. RESULTS AND DISCUSSION

This part is dedicated to quantitative and qualitative analyses of the numerical study. Results are compared with the experimental data base of Morelli [7].

6.1 Global performance predictions

A comparison of the numerical predictions with the bench test data is carried out on Figure 8 a) and b). The global thrust of the Fenestron® as well as the shroud and the rotor thrust are presented. Compared to the test bench measurements, the function point at a blade pitch angle of +35° is reached for both RANS and LES calculations. The total thrust is equally shared between rotor and shroud thrusts. On the thrust-power polar, Figure 8 b), a power deficit is observed. An error of 20% is noted between the numerical simulation and the experimental test. The influence of the numerical scheme on the thrust-power prediction has been previously highlighted [10]. The power deficit here can be attributed to the second-order JST scheme.

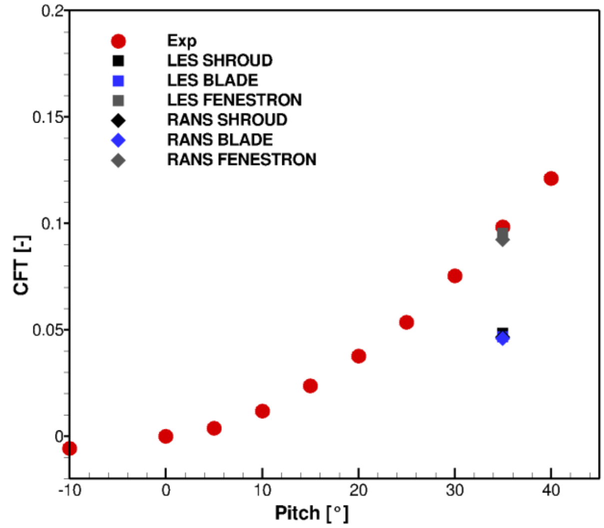

a) ***Fenestron® CFT-Pitch Polar***

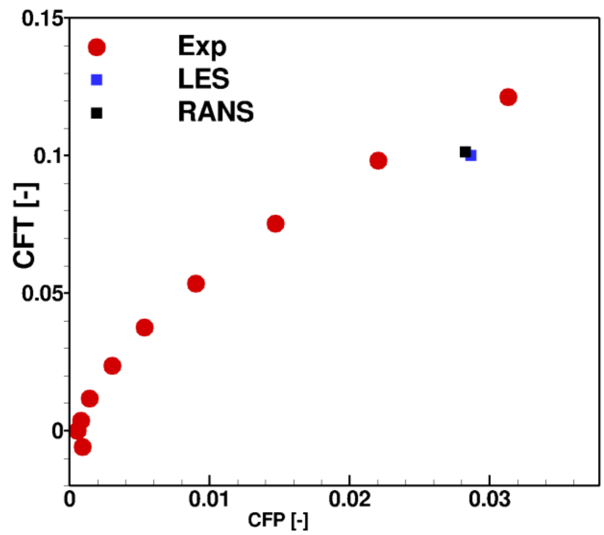

b) Fenestron® CFT-CFP Polar

Figure 8: Influence of the computational approach on the global performance

6.2 Local performance predictions

An analysis of the local performance of the shroud and the blade is carried out for both approaches. For RANS and LES solutions, an azimuthal averaging was performed. In addition, for LES approach, a time average of 2 revolutions is considered.

Figure 9 presents the pressure-coefficient profile through the vein.

From A to B: The upper collector zone evolves in a low-pressure area, where the suction peak is reached at the maximal curvature radius. This region of the shroud generates most of the shroud thrust. Compared to bench test data, the RANS approach accurately describes the

pressure distribution in the collector area. The LES overestimates the pressure coefficient. In the case of RANS simulation, the flow is considered as fully turbulent, whereas a laminar-turbulent transition is observed at the end of the collector with the LES solution.
From B to C: In the blade region, a suction peak is related to the presence of the blade tip vortices. Compared to the RANS modelling, the LES approach improves the suction peak prediction. Such a suction peak has already been reported in the literature [5][10]. However, since this part of the shroud is parallel to the rotational axis, it does not affect the global shroud thrust.
From C to D: In the diffuser part, the pressure returns to the ambient static pressure value. Both approaches correctly predict the pressure recovery.

Figure 10 a) (respectively b)) presents the radial profile of the normalized axial velocity downstream the rotor (plane 2) (respectively at the end of the vein (plane3)).
Plane 2: Figure 10 a) highlights the influence of the LES on the blade-tip prediction just behind the rotor. The RANS overestimates the axial velocity whereas the LES improves the prediction in the vicinity of the tip gap. In the linear zone, from h/H=0.2 to h/H=0.8, both RANS and LES predict the same trend.
Plane 3: Figure 10 b) illustrates the influence of the method to propagate wakes. In the linear part of the vein, LES and RANS give the same results. From h/H=0 to h/H=0.2, the blade-root vortex is propagated to the end of the vein for both approaches. The blade-tip vortex flow appears at h/H=0.8. Its position is accurately predicted by the LES approach in comparison with the experimental data. The radial velocity profile highlights the displacement of the two extremity vortices. The blade-root vortex is carried up into the vein whereas as a mirror the tip leakage flow is carried down into the vein.

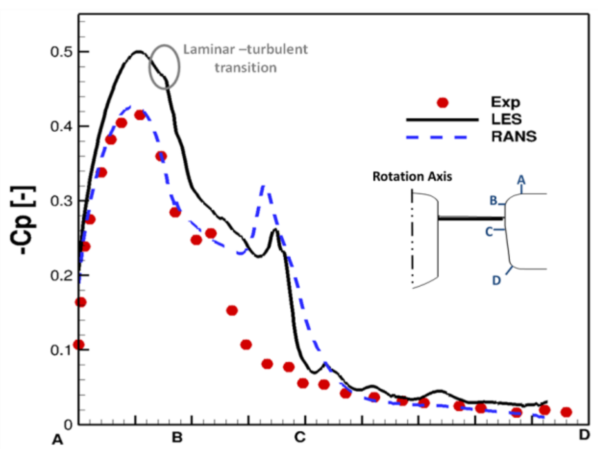

Figure 9 : Pressure coefficient distribution on the shroud

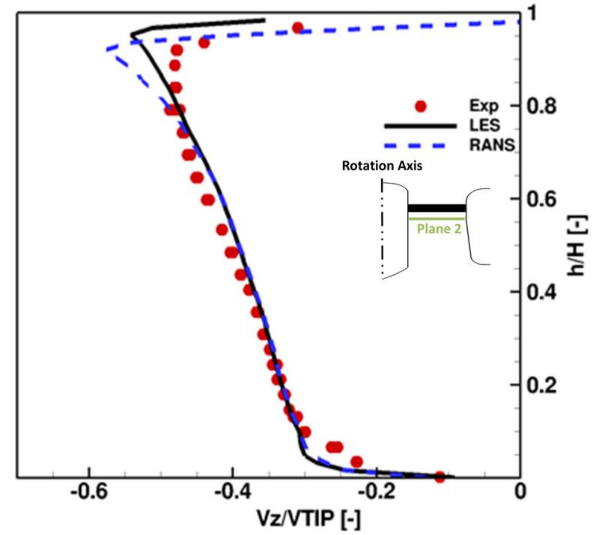

a) Plane 2

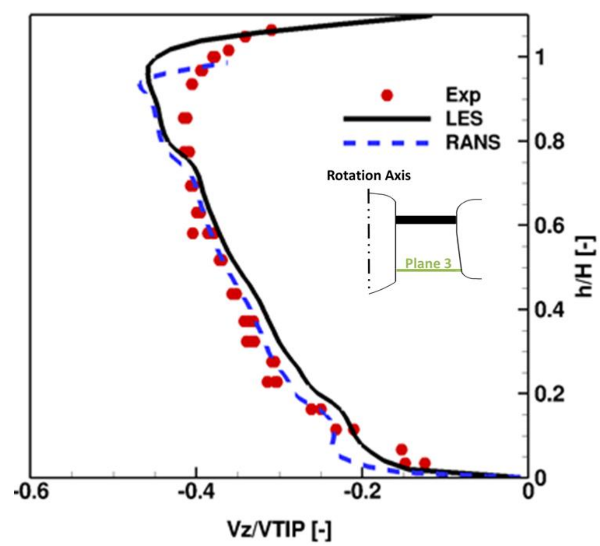

b) Plane 3

Figure 10 : Axial-velocity distribution in the vein

6.3 Qualitative comparison between the two approaches

It is here proposed to analyze the flow in the vicinity of the blade tip. First observations on the wake propagation between RANS and LES are carried out on a radial slice at h/H=0.8. Then, it is proposed to characterize the flow in this region by using the Q-criterion [31] in order to identify the vertical structures. Vortices are identified with a positive Q-criterion, which highlights areas of the fluid domain where the vorticity magnitude is greater than the deformation.

Figure 11 presents the pressure field inside the vein at h/H=0.8. Between the two solutions, the topology of the flow is similar. On the suction side, the pressure recovery appears at 50% of the blade profile. Discrepancies appear on the pressure side.

For both approaches, the wake is well preserved through the vein. In the case of LES calculation, wake flow patterns are resolved whereas a smooth wake is predicted by the RANS solution.

Figure 12 presents iso-surfaces of positive Q-criterion colored by the non-dimensioned velocity Vz/Vtip. It is here proposed to discuss about discrepancies observed between RANS and LES solutions.

Collector region:

At the end of the collector, a separation zone was observed on a previous work with a RANS approach [10]. A similar flow behavior is observed in the present RANS solution (Figure 12 a)). In the case of LES, a laminar-turbulent transition occurs and is pointed out on Figure 12 b). This separation can explain discrepancies observed on the pressure-coefficient profile.

Blade-root part: h/H=0 to h/H=0.2

Differences in vertical resolution are important between RANS and LES approaches. Near the blade-root region, for both approaches, a horse-shoe vortex is generated. It separates into two arms at the leading edge of the blade-root, one directed to the pressure side of the blade and one to the suction side of the blade. It interacts with the blade root trailing edge vortex. The size of the global vortex depends on the blade-root geometry.

Linear blade region: h/H=0.2 to h/H=0.8

In the linear region of the blade, the LES approach highlights a laminar-turbulent transition zone at 25% of the chord. The position of the boundary-layer transition depends on the blade radius. Increasing the axial velocity delays the transition as it can be observed on Figure 12. It is the first time that a transition is observed on a Fenestron® configuration. Similar results, in the turbomachinery field, are observed on a shrouded rotor at equivalent Reynolds number [32]. Moreover, numerous structures, at the blade trailing-edge, are clearly seen in the LES solution.

Blade-tip region: h/H=0.8 to h/H=1

In this region, two flow mechanisms interact. First, the blade-tip vortex is generated by the tip clearance, close to the shroud. Then, the boundary layer of the shroud interacts with this vortex, leading to a secondary flow. The blade tip vortex sucks the boundary-layer of the shroud which leads to a pressure drop on the shroud. Global structures are clearly different between the RANS and LES approaches, which lead to two blade-tip mechanisms.

It is proposed, here, to analyze the two blade-tip mechanisms described on Figure 13. In the case of RANS solution, Figure 13 a), a primary vortex from the upper edge is generated. It is driven by the rotation into the vein. Secondary vortices from the lower edge of the blade are feeding the first vortex. Then the blade trailing edge vortex is deviated into the primary vortex. Vortices roll-up into a large structure which name is the tip-leakage flow and is convected into the vein.

In the case of LES solution, Figure 13 b), two vortices are generated from the leading edge of the profile. A first vortex is generated from the upper edge nearby the leading edge. A second vortex appears from the lower edge in the vicinity of the leading edge. Then, at 25% of the chord, the lower vortex rolls-up into the upper edge and generates the tip-leakage flow. Figure 14 presents a zoom of the Q-criterion in the vicinity of the blade. A preliminary vortex appears at the suction side of the profile. It is deviated directly into the vein. As it is not feeding by the vorticity, it disappears. In addition, the interaction between the tip leakage flow and the boundary layer transition is pointed out on Figure 13 b) and Figure 14. When the boundary-layer transition occurs, the tip vortex detaches from the profile and is convected downstream into the vein.

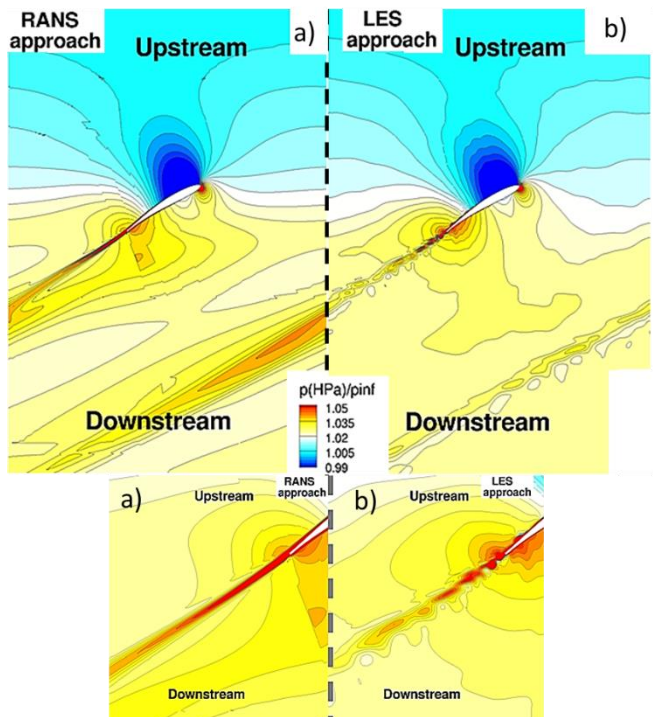

Figure 11 : Instantaneous pressure fields at h/H=0.8 – a) the RANS approach and b) the LES approach

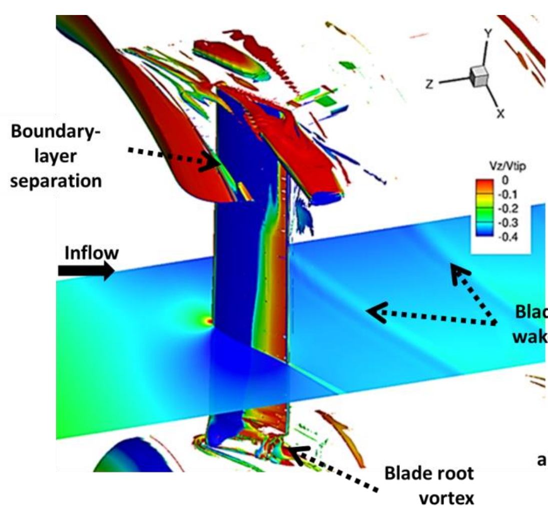

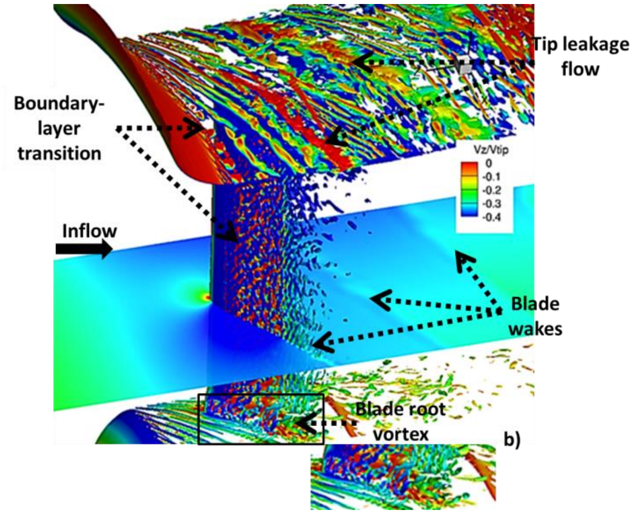

Figure 12 : Instantaneous turbulent structures inside the vein of the Fenestron® – Q-criterion coloured by the Vz/Vtip for RANS approach a) and LES approach b)

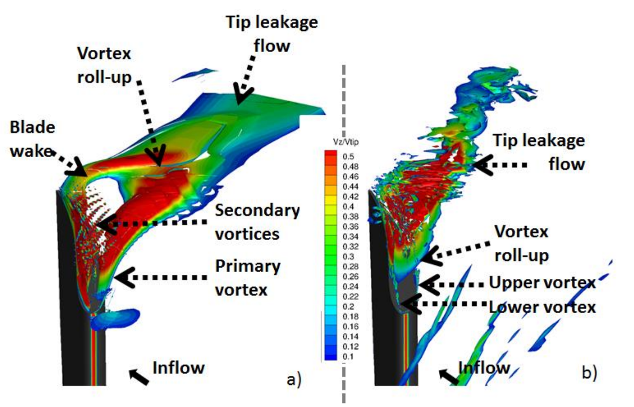

Figure 13 : Instantaneous turbulent structures near the blade tip – Q-criterion coloured by the Vz/Vtip for RANS approach a) and LES approach b)

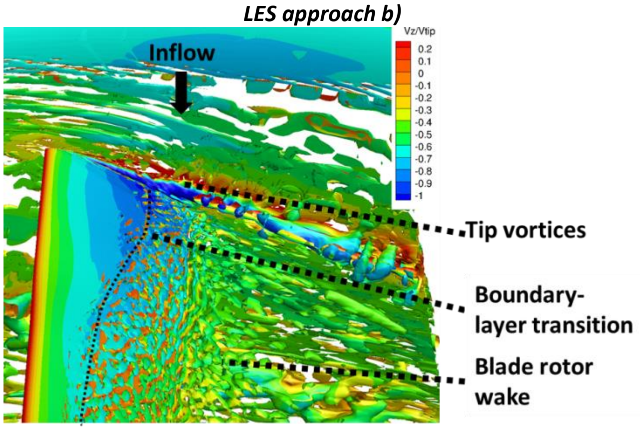

Figure 14 : Instantaneous iso surface of Q-criterion colored by Vz/Vtip – focus on the vicinity of the blade tip for LES simulation

7. Conclusion

A first Large Eddy Simulation has been carried out on the Fenestron® geometry. To be compliant with meshing standard for LES, the blade passage model is meshed using no-match planes inside the vein.

A comparison between a classical RANS modelling and the LES approach was conducted on global and local performance of the Fenestron®. There is no influence of the turbulence resolution on the pitch-thrust and on the power-thrust polars. For both approaches, results are in good agreement with experiments. Nevertheless, local comparisons of performance highlighted discrepancies. In the vicinity of the blade, as it was expected, the turbulence has a strong influence on the tip leakage flow. Differences were pointed out on blade velocity profiles just behind the rotor. The LES approach seems to accurately predict the tip leakage flow where the RANS model overestimates the axial velocity in this region. Nevertheless, a high magnitude of the pressure coefficient is predicted by the LES approach in the collector area. It is here, first results of LES investigations on a Fenestron® configuration.

Qualitative investigations pointed out the laminar-turbulent transition on the rotor. The LES brings a better understanding of the interaction between the shroud and the rotor. A first description of the tip-leakage flow of the Fenestron® is given. A dependency between the blade-tip vortex and the laminar-turbulent transition is highlighted.

Future investigations can concerns the experimental data base and particularly the surface condition of the shroud. Regarding the interaction between fixed (shroud) and rotating parts (rotor), a complete geometry of the Fenestron® should be computed to highlight the influence of the other fixed parts as the stator and the vertical tail fin on the flow of the Fenestron®.

REFERENCES

[1] Mouille, R., Bourdaquez, G., " Helicopter steering and propelling device", patent, 1.511.006, April 1970

[2] Mouille, R., "Ten years of Aerospatiale experience with the Fenestron and conventional tail rotor", 35th annual national forum of the American Helicopter Society, Washington D.C., USA, May, 1979

[3] Gourdain, N., and Wlassow F., and Ottavy, F., "Effect of tip clearance dimensions and control of unsteady flows in a multi stage high pressure compressor", Journal of Turbomachinery 134, 051005 (DOI:10.1115/1.4003815)

[4] Wright, G., and Nickerson, J., "HANDLING QUALITIES OF THE H-76 FANTAILTM DEMONSTRATOR", 47^{th} AHS, 1991

[5] Rajagopalan, R. Ganesh, and Keys, C. N., "Detailed Aerodynamic Design of the RAH 66 FANTAIL USING CFD", American Helicopter Society 49th Annual Forum Proceedings, St Louis, Missouri, USA, May 1993

[6] Gardarein, P., Canard, S., and, Prieur, J., "Unsteady aerodynamic and aeroacoustic simulations of a Fenestron® tail rotor", 62th Americain Helicopter Society, Phoenix, Arizona, USA, May 9-11, 2006

[7] Morelli, F., Vuillet, A., "New Aerodynamic Design of the Fenestron® for Improved Performance", 12th European Rotorcraft Forum, Amsterdam, Netherland, September, 1986

[8] Morelli, F., and Vuillet, A., " Le Fenestron® sur l'hélicoptère", 19ième colloque d'aérodynamique appliquée, Marseille, France, Novembre 1982

[9] Kainz, M., and LE Chuiton, F., « Numerical investigation into the unsteady aerodynamics of a ducted helicopter tail rotor under side wind conditions », ASME Turbo Expo, Glassgow, UK, 2010

[10] Marino, M., and Gourdain, N., and Legras, G., and Alfano, D., " Aerodynamic simulation strategies assessment for a Fenestron® in hover flight ", 6th EUCASS, Krakow, Poland, 2015

[11] Alpman, E., Long, Lyle N., and Kothmann, Bruce D., "Unsteady RAH-66 Comanche flowfield simulations", presented at the American Helicopter Society 59th Annual Forum, Phoenix, Arizona, USA, May 2003

[12] Gardarein, P., and Falissard, F., and Binet, L., and Camus, J-C., "Validation of aerodynamic and aeroacoustic computations of a Fenestron® in real flight conditions", 36th European Rotorcraft Forum, Paris, France, 2010

[13] Mouterde, E., Suder, L., Dequin, A.M., D'Alascio, A., Haldenwang. P., "Aerodynamic computations of isolated Fenestron® in hover conditions", 33th European Rotorcraft Forum, Kazan, Russia, September, 2007

[14] D'Alascio A., Le Chuiton F., Mouterde E., Sudre L., Kirstein S., and Kau, H.-P., " Aerodynamic study EC135 FEN HFC By means CFD", presented at the American Helicopter Society 64th Annual Forum, Montréal, Canada, 29 April-1 May, 2008

[15] You, J., and Breitsamter, C., "Numerical investigation of aeroacoustic sound sources in Encapsulated Helicopter Tail Rotor", AIA-DAGA, 2012

[16] Chaderjian, Neal M., and Ahmad, Jasim U., "Detached Eddy Simulation of the UH 60 Rotor Wake Using Adaptive Mesh Refinement", 68th AHS, Fort Worth, Texas, May, 2012

[17] Lombard, J.-E. W., Moxey, D., Hoessler, J. F. A., Dhandapani, S., Taylor, M. J., and Sherwin, S. J., "Implicit Large Eddy Simulation of a Wingtip Vortex at Rec=1.2.10^{6}", Physics.flu.dyn, 2007, ArXiv ID:1507.06012

[18] Gourdain, N., "Validation of large-eddy simulation for the prediction of compressible flow in an axial compressor stage", ASME turbo Expo, 2013, GT2013-94550

[19] Denton, J., "Some limitations of Turbomachinery CFD", ASME turbo Expo 2010, Power for Lanc Sea and Air, volume 7: Turbomachinery, Parts A, B and C, Glasgow, UK, June 14-18, 2010, ISBM 978-0-7918-4402-1.

[20] Kok,J., "Improvements of the Two equation Turbulence Models in Multi-Block Flow Solvers : Free-Stream Dependancy and Transition", Rapport technique, AVTAC/TR/NLR/JCK990520/Draft2, 1999

[21] Menter, F.R., "Zonal two equation k-omega Turbulence models for aerodynamic flows", AIAA paper 93-2906 Proc 24th Fluid Dynamics Conference

[22] Spalart, P.R., "Strategies for turbulence modelling and simulations", Int J Heat Fluid Flow, 2000, DOI:2000;21.525-63

[23] Piomelli, U., "Wall layer models for large-eddy simulations", Progress in Aerospace Sciences, 2008 DOI:10.1016/j.paerosci.2008.06.001

[24] Chapman, D.R, "Computational aerodynamics development and outlook", AIAA J, 1979, DOI:1979;17;1293-313

[25] Nicous, F., and Ducros, F., "Subgrid-scale stress modelling based on the square of the velocity gradient tensor", Flow Turbulence and Combustion, April 1999

[26] Cambier, L., Heib, S., and Plot, S. "The Onera elsA CFD Software: Input From Research and Feedback From Industry", Mechanics & Industry, Vol. 14, No. 3, 2013, pp. 159-174, doi:10.1051/meca/2013056.

[27] Jameson, A., Schmidt, W., and Turkel, E., "Numerical Solution of the Euler Equations by Finite Volume Methods Using Range Kutta Time-Stepping Schemes", AIAA Paper 198-1259, 14th Fluid and Plasma Dynamics Conference, June 1981, doi : 10.2514/6.1981-1259

[28] Desvigne, D., Marsden, O., Bogey, C. & Bailly, C., 2010, Development of non-centered wavenumber-based optimized interpolation schemes with amplification control for overlapping grids, SIAM Journal on Scientific Computing,32(4), 2074-2098.

[29] Youn, S., and Jameson, A., "An LU-SSOR Scheme for the Euler and Navier-Stokes Equations", AIAA 25th Aerospace Sciences Meeting, Paper No. 87-0600, Reno, NV, USA.

[30] Jameson, A., "Tie Dependant Calculation Using Multgrid with Applications to Unsteady Flows Past Airfoils and wings", 10th AIAA Computational Fluid Dynamics Conference, Paper No 91-1596, 1991

[31] Jeong J. and Hussain F., "On the identification of a Vortex", Journal of Fluid Mechanics, Vol 285, 1995, pp 69-94, doi 10.1017/S0022112095000462.

[32] Wang, G., Moreau, S., Moreau, S, Duchaine, F., Laborderie, J., Gicquel, L., "LES investigation of Aerodynamics Performance in an axial Compressor Stage", 22nd Annual Conference of the CFD Society of Canada, Toronto, Canada, 2014